Measuring spatially varying, multispectral, ultraviolet bidirectional reflectance distribution function with an imaging spectrometer

Hongsong Li
Hang Lyu
Ningfang Liao
Wenmin Wu

SPIE.

Measuring spatially varying, multispectral, ultraviolet bidirectional reflectance distribution function with an imaging spectrometer

Hongsong Li,[a,*] Hang Lyu,[b] Ningfang Liao,[b] and Wenmin Wu[b]
[a]Beijing Institute of Technology, School of Software Engineering, Key Laboratory of Digital Performance and Simulation Technology, No. 5, South Zhongguancun Street, Haidian District, Beijing 100081, China
[b]Beijing Institute of Technology, School of Optoelectronics, Key Laboratory of Photoelectronic Imaging Technology and System, Ministry of Education of China, No. 5, South Zhongguancun Street, Haidian District, Beijing 100081, China

Abstract. The bidirectional reflectance distribution function (BRDF) data in the ultraviolet (UV) band are valuable for many applications including cultural heritage, material analysis, surface characterization, and trace detection. We present a BRDF measurement instrument working in the near- and middle-UV spectral range. The instrument includes a collimated UV light source, a rotation stage, a UV imaging spectrometer, and a control computer. The data captured by the proposed instrument describe spatial, spectral, and angular variations of the light scattering from a sample surface. Such a multidimensional dataset of an example sample is captured by the proposed instrument and analyzed by a *k*-mean clustering algorithm to separate surface regions with same material but different surface roughnesses. The clustering results show that the angular dimension of the dataset can be exploited for surface roughness characterization. The two clustered BRDFs are fitted to a theoretical BRDF model. The fitting results show good agreement between the measurement data and the theoretical model. © *The Authors. Published by SPIE under a Creative Commons Attribution 3.0 Unported License. Distribution or reproduction of this work in whole or in part requires full attribution of the original publication, including its DOI.* [DOI: 10.1117/1.OE.55.12.124106]

1 Introduction

The bidirectional reflectance distribution function (BRDF) data in the ultraviolet (UV) band are valuable for many applications. However, measuring BRDF in the UV band is in general a difficult task. The challenges are multifold: the choices of the detectors and the light sources are scarce; the strong chromatic aberration of the transmissive optics lowers the data quality; the reference sample or the reference light source in UV band requires spectral and photometric calibration, etc. To obtain multispectral/hyperspectral measurement, data in UV band adds more complication to the design of such a measurement instrument.

Measuring BRDF has long been considered a time-consuming task since BRDF data have one spectral dimension and up to four angular dimensions (depending on the surface characteristics). One common approach to improve the efficiency of the measurement instrument is to use an imaging device as the detector, which captures two-dimensional intensity data with one snapshot. The setup makes it possible to measure spatially varying BRDF (SVBRDF). In recent years, the development of the multispectral/hyperspectral imaging technology has provided new imaging devices in the UV band, such as the UV imaging spectrometers.[1–3] Such an instrument is capable of capturing images with good spatial and spectral resolution in near- and middle-UV bands.

In this paper, we present a BRDF measurement instrument equipped with a broadband UV light source and a UV imaging spectrometer. The presented instrument is able to capture the reflected light energy of a flat sample surface from various incidence angles and in multiple wavelengths of a UV band. A calibration method is proposed to convert the captured signal to the BRDF.

2 Related Works

A few BRDF measurement instruments working in the UV band are documented. In 1993, National Institute of Standards and Technology reported a reference spectrophotometer for reflectance in the near-UV band.[4] TMA Technologies Inc. reported a broadband scatterometer that allows measurements from 250 to 900 nm.[5] These instruments are equipped with a Xenon arc source and a monochromator as the UV light source. Later, BRDF measurements in the EUV band were presented by several works.[6–8] The need for EUV BRDF data arises primarily in the area of stray light design and analysis. Due to the strong scattering of air in the EUV band, a vacuum chamber is usually required for such an instrument. Schröder et al.[9] present an angle-resolved scattering and reflectance measurement instrument working at a 13.5-nm wavelength to inspect the surfaces of optical components. Georgiev and Butler[10] presented long-term calibration monitoring of BRDF for Spectralon® diffuser samples ranging from 230- to 450-nm wavelengths. Bai et al.[11] built an angle-resolved BRDF measurement system and the obtained measurement data cover the UV wavelengths ranging from ∼250 to 370 nm and several incidence angles. Most of the above-mentioned instruments are equipped with a spectrometer in the UV band as the detector. Nevertheless, there is no instrument documented using an imaging spectrometer as the detector, and no SVBRDF data have been reported.

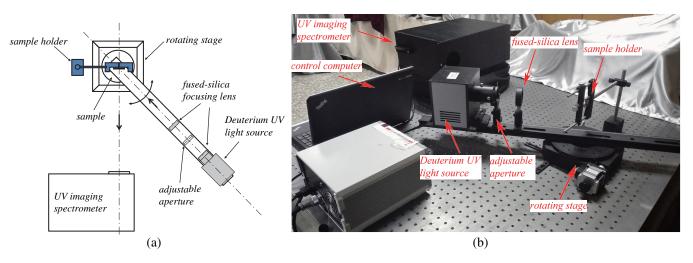*Address all correspondence to: Hongsong Li, E-mail: lihongsong@bit.edu.cn

Fig. 1 UV BRDF measurement system: (a) system overview and (b) the actual setup.

Modeling BRDF in the UV band specifically is not necessary in general. Most of the BRDF models based on the geometrical optics or the wave optics work well in the UV band. However, strong volume scattering and retro-reflection can be observed in the UV band for certain materials. In this case, a BRDF model to describe such characteristics is needed. Based on the measurement data presented in Ref. 11, Bai et al. proposed a seven-parameter statistical BRDF model incorporating surface scatter, volume scatter, and retro-reflections. Later, Bai et al.[12] modeled the spectral scattering characteristics of a space target in near-UV to visible bands (300 to 800 nm) based on a BRDF model modified from the Davis BRDF Model.

Since late 1990s, the image-based BRDF measurement has become popular, especially in the computer graphics and computer vision communities.[13–17] Dana et al.[13] introduced measurement equipment that captures the reflection from a spatially varying material from a range of viewing/illumination directions by a video camera. Although the camera has limited spectral coverage (3 channels) and limited dynamic range (8/12 bits), it demonstrates great potential as a photometric detector matrix.

Multispectral imaging captures the spatial reflectance mapping by combining spectroscopes and digital image of the sample surfaces. The multispectral imaging data are in the form of an image cube with two spatial dimensions and one spectral dimension, sampled over a discrete number of wavelength intervals. Multispectral imaging in the UV band reveals interesting characteristics of the sample surface that are invisible in visible band[18] and are applied to analyze traces of blood,[19] explosives,[20] and fingerprints.[21] However, multispectral image data at one (or several) angular configuration are sometimes insufficient, especially when the materials of interest have different roughness characteristics and similar spectral characteristics. In these cases, it is a challenge to distinguish these materials by only analyzing their spectra. By combining multispectral imaging with angularly resolved reflectometry, we are able to analyze the light scattering from a sample surface from the spatial, spectral, and angular dimensions. We expect that adding angular dimension into the data could widen the application scope of the multispectral imaging technology.

3 System Design

An overview and the actual setup of the proposed system are illustrated in Fig. 1. The proposed instrument consists of four parts: a broadband collimated UV light source, a positioning mechanism including a rotation stage and a sample holder, a UV imaging spectrometer, and a computer system [not shown in Fig. 1(a)] for data acquisition and instrument control.

The ideal light source for the proposed system would have a strong emission across the near- and middle-UV bands (200 to 400 nm) and be collimated. We chose a deuterium UV lamp for broad spectral coverage in the UV band. The lamp provides a continuous spectrum in the desired UV range with higher output in the shorter wavelength side. The lamp is equipped with a housing and a fused silica lens that gather the output beam. The lens can be adjusted along the optical axis to vary the focus. To provide a collimated incident light beam, an adjustable aperture and the second fused silica lens are added. The aperture is positioned at the foci of both fused silica lenses. A UV CCD camera (FLI PL4710) is used to examine the uniformity and symmetry of the light spot of the finished light source set on a flat, uniform surface. The resulting beam is well collimated: it has a solid angle of $\sim 2 \times 10^{-3}$ sr, with illumination uniform to within $\pm 5\%$ over a circular region of 20-mm diameter. The two fused silica lenses filter out a portion of the UV light emission, reducing the output spectrum at the shorter wavelength side. The spectrum of the light source set is measured by a fiber spectrometer (Ocean HR4000). The setup of the light source set and the output spectrum is presented in Fig. 2. However, the photometric calibration of this light source set is not included in this work. Thus, the intensity given in Fig. 2 is uncalibrated reading values obtained by the fiber spectrometer.

The light source is mounted on an optical rail of 100-cm length, which is attached to a rotation stage. This optical rail rotates in a horizontal plane (parallel to an optical table). The angular resolution of the rotation stage is 0.1 deg. A sample holder is mounted on the optical table and carefully aligned to the detector. The light scattering of the sample holder in the UV band is examined by the UV CCD and no obvious stray light can be detected. This setup allows us to vary the
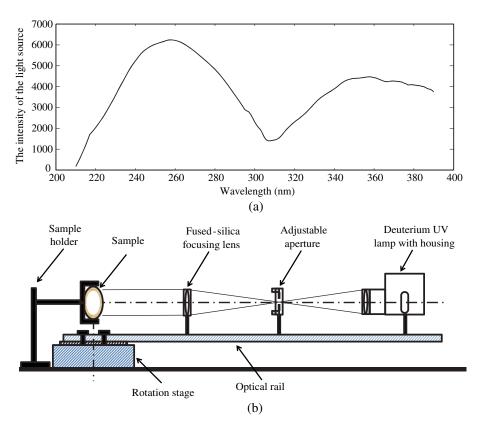
Fig. 2 The collimated UV light source: (a) the output spectrum of the broadband UV light source and (b) the overview of the broadband UV light source.

incidence angle for BRDF measurement and obtain in-plane BRDF data. In the future, a two-axis rotation stage can be added as the sample holder to cover the entire reflection hemisphere. Some sampling positions (within ∼12 deg of retro-reflection) are not achievable, due to the occlusion of the light source and the imaging spectrometer. We omit such positions and apply interpolation to fill gaps in data as needed.

The imaging spectrometer consists of an oscillating mirror, a Cassegrain objective, a Michelson structure, an Offner relay, and a UV-enhanced CCD (an FLI PL4710). The details of this instrument are presented in Ref. 3. A multilayer dielectric film is coated onto the oscillating mirror to filter out the visible light and to reduce the polarization effect. The imaging spectrometer is able to obtain ∼100 wavelength samples over the range of 240 to 370 nm. A strong absorption around the 290-nm wavelength is discovered, mainly caused by the optical glue at the beam-splitter. Thus, the working band of this instrument becomes 240 to 285 nm and 295 to 370 nm. The field of view of the image spectrometer is ∼2.5 deg. For each pixel, the solid angle of incident light is then 0.0025 deg so that the angular resolution is 0.04 mrad. The small solid angle of the detector is ideal for BRDF measurement. At the designed target distance of 700 mm, the spatial resolution is ∼29.30 μm. A control computer coordinates all the components of the imaging spectrometer and automatically captures a series of images. Then the images are reconstructed into an interferogram datacube, given as $I(x, y, \delta)$. By the Fourier transformation, $I(x, y, \delta)$ can be converted into a spectrum datacube, given as $I(x, y, \nu)$, in which ν is the wavenumber. The scanning scope

and the exposure time of the imaging spectrometer can be adjusted by the control software. A typical scan of a 20-mm-wide sample surface and 0.5 s per frame exposure time takes ∼450 s to obtain one interferogram datacube. At the grazing angle of reflection, the exposure time for BRDF measurements could be considerably longer.

4 System Calibration

Accurate BRDF measurement requires the spectral and photometric calibrations for both the light source and the detector. In our work, the spectral response of the imaging spectrometer is determined first. Next, the rest of the measurement system is calibrated as one instrument parameter curve. This is equivalent to a relative measurement method to obtain BRDF.

The spectral calibration of the imaging spectrometer is needed since we need to determine the actual wavelength for each sample in the ν dimension of $I(x, y, \nu)$. The detail of this spectral calibration is presented in Ref. 3. Here, we only give a brief introduction of this step. A high-pressure mercury lamp, which has a characteristic peak at 365.0 nm (27,388.3 cm^{-1} in wavenumber) in its output spectrum, is used as the reference for spectral calibration. As explained in Ref. 3, a light source with a single peak at a known wavelength is sufficient for accurate spectral calibration. A sample with a uniform surface (a white ceramic sample) is illuminated and the reflected light is captured by the imaging spectrometer with one snapshot. The captured image shows a uniformly distributed fringe. Then the spectrum is calculated by spectral inversion algorithm based on the Fourier transformation. The calibration results of the
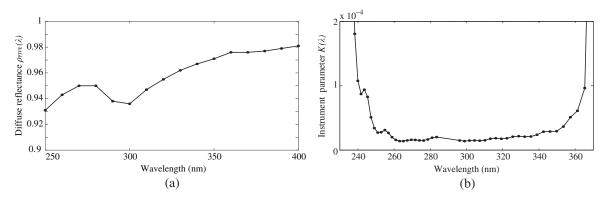
Fig. 3 Determining the instrument parameter: (a) The measured diffuse reflectance $\rho_{\mathrm{PTFE}}(\lambda, 10\ \mathrm{deg})$ and (b) the obtained instrument parameter $\kappa(\lambda)$.

imaging spectrometer then give correct wavelengths to the spectrum dimension of the spectrum datacube $I(x, y, \nu)$. The spectral resolution varies with the wavelength, which is 0.90 nm at 240 nm and 2.13 nm at 370 nm.

Assuming the light source and the imaging spectrometer have stable performance during the measurement, we apply a relative method for BRDF normalization. The radiance dL_r reflected from the sample surface can be written as

$$dL_r(\lambda; \theta_i, \varphi_i; \theta_r, \varphi_r) = \kappa_1(\lambda)\frac{V(\lambda; \theta_i, \varphi_i; \theta_r, \varphi_r)}{t}, \qquad (1)$$

where $\kappa_1(\lambda)$ is the spectral response of the imaging spectrometer, which is a function of the photometric response of the CCD, spectral transmittance of the optical system, the solid angle of the pixel, the size of the pixel, etc., $V(\lambda; \theta_i, \varphi_i; \theta_r, \varphi_r)$ is the spectral signal at each pixel, and t is the exposure time.

Assuming a stable light source output, the irradiance on the sample surface $dE_i(\lambda; \theta_i, \varphi_i)$ is only a function of θ_i and can be written as $dE_i(\lambda; 0 \times \mathrm{deg}, 0 \times \mathrm{deg}) \cos \theta_i$. $dE_i(\lambda; 0 \times \mathrm{deg}, 0 \times \mathrm{deg})$ is the irradiance of normal incidence, which is a constant by assuming a stable light source output and constant distance between the light source and the sample surface. Thus, the BRDF can be written as

$$\begin{aligned} f_r(\lambda; \theta_i, \varphi_i; \theta_r, \varphi_r) &= \frac{dL_r(\lambda; \theta_i, \varphi_i; \theta_r, \varphi_r)}{dE_i(\lambda; \theta_i, \varphi_i)} \\ &= \frac{\kappa_1(\lambda)}{dE_i(\lambda; 0\ \mathrm{deg}, 0\ \mathrm{deg})}\frac{V(\lambda; \theta_i, \varphi_i; \theta_r, \varphi_r)}{t \cos \theta_i} \\ &= \kappa(\lambda)\frac{V(\lambda; \theta_i, \varphi_i; \theta_r, \varphi_r)}{t \cos \theta_i}, \qquad (2)\end{aligned}$$

where $\kappa(\lambda)$ is the instrument parameter for the proposed instrument, combining the spectral and photometric characteristics of both the light source and the imaging spectrometer.

To determine this instrument parameter $\kappa(\lambda)$, a reference sample with known BRDF needs to be measured by our instrument. In our work, we choose a piece of flat polytetrafluoroethylene (or PTFE) panel as the reference sample. The diffuse reflectance $\rho_{\mathrm{PTFE}}(\lambda, 10\ \mathrm{deg})$ of this reference sample is measured at 10 deg incidence by the National Institute of Metrology, China. With less than 1.0% uncertainty, the measured diffuse reflectance $\rho_{\mathrm{PTFE}}(\lambda, 10\ \mathrm{deg})$ has ~5% variations (0.93 to 0.98) over the wavelength range of 250 to 370 nm, as shown in Fig. 3(a). Unfortunately, we are unable

to obtain BRDF data at <12 deg incidence due to the occlusion of the detector and the light source. As the scattering characteristic of the reference sample is determined mainly by its strong subsurface scattering, slight variations of the incidence angles (5 deg) have little influence on its BRDF and diffuse reflectance, as long as the incidence angle is $\leq$20 deg.[22] Thus, the BRDF at 15 deg incidence is measured. Assuming $\rho_{\mathrm{PTFE}}(\lambda, 10\ \mathrm{deg}) \approx \rho_{\mathrm{PTFE}}(\lambda, 15\ \mathrm{deg})$ and the reference sample has a Lambertian surface

$$\begin{aligned} \rho_{\mathrm{PTFE}}(\lambda, 10\ \mathrm{deg}) &\approx \rho_{\mathrm{PTFE}}(\lambda, 15\ \mathrm{deg}) \\ &\approx \pi f_{r,\mathrm{PTFE}}(\lambda; 0\ \mathrm{deg}, 15\ \mathrm{deg}; 0\ \mathrm{deg}, 0\ \mathrm{deg}) \\ &= \pi\kappa(\lambda)\frac{V_{\mathrm{PTFE}}(\lambda; 15\ \mathrm{deg}, 0\ \mathrm{deg}; 0\ \mathrm{deg}, 0\ \mathrm{deg})}{\cos 15\ \mathrm{deg}}, \qquad (3)\end{aligned}$$

where $\rho_{\mathrm{PTFE}}(\lambda, 15\ \mathrm{deg})$ is the diffuse reflectance of the PTFE sample at 15 deg incidence, $f_{r,\mathrm{PTFE}}(\lambda; 0\ \mathrm{deg}, 15\ \mathrm{deg}; 0\ \mathrm{deg}, 0\ \mathrm{deg})$ is the measured BRDF at (15 deg, 0 deg; 0 deg, 0 deg), and $V_{\mathrm{PTFE}}(\lambda; 0\ \mathrm{deg}, 15\ \mathrm{deg}; 0\ \mathrm{deg}, 0\ \mathrm{deg})$ is the spectral signal obtained by measuring the PTFE sample by the imaging spectrometer. Thus, we have

$$\begin{aligned} &\rho_{\mathrm{PTFE}}(\lambda, 10\ \mathrm{deg}) \\ &\approx \pi\kappa(\lambda)\frac{V_{\mathrm{PTFE}}(\lambda; 15\ \mathrm{deg}, 0\ \mathrm{deg}; 0\ \mathrm{deg}, 0\ \mathrm{deg})}{\cos 15\ \mathrm{deg}}. \qquad (4)\end{aligned}$$

With Eq. (4), we then calculate $\kappa(\lambda)$ at various sampling wavelengths. $\rho_{\mathrm{PTFE}}(\lambda, 10\ \mathrm{deg})$ at these sampling wavelengths are obtained by interpolation. The obtained $\kappa(\lambda)$ is shown as the black dots in Fig. 3(b). Figure 3(b) shows small variations except at both sides of the spectra, where the bandpass film of the oscillating mirror in the imaging spectrometer filters out the spectral signal V_{PTFE} at these wavelengths.

Now, without the photometric calibration of both the light source and the imaging spectrometer, we are able to relate the measured spectrum $V(\lambda)$ to the spectral BRDF value $f_r(\lambda)$ through $\kappa(\lambda)$ as given in Eq. (3).

5 Experiment Results

5.1 Measurement Data

To illustrate the capability of the proposed instrument, we measure the spectral BRDF of an example sample with spatially varying material. The back of an iPad is chosen as
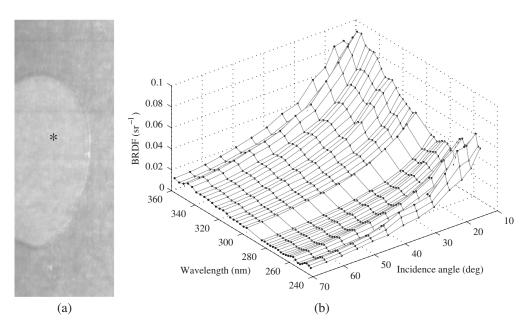
Fig. 4 An example of BRDF measurement data of iPod shuffle sample: (a) the image of the sample surface at $\lambda = 300$ nm and $\theta_i = 18$ deg and (b) the obtained spectral BRDF data on asterisk.

the sample surface for the BRDF measurement. The surface is made of an aluminum alloy and has an Apple logo on it. The logo is visible because it is slightly rougher than the base surface. Since the entire sample surface is quite smooth, the BRDF data in the visible spectrum must have a large dynamic range in the vicinity of the specular reflection direction. The analysis of its surface roughness from its BRDF data can be challenging. Usually, a traditional gonioreflectometer equipped with a single photoelectronic detector is more suitable to capture the reflection intensity with such a large dynamic range. In the UV spectrum, the BRDF of this sample has a relatively smaller dynamic range and is easier to capture by an image-based measurement method. Our goal is to obtain the spectral SVBRDF data of this sample, to use the data to separate the surface regions with different roughness characteristics, and to characterize the two surface regions.

The spectral images of the central part of the sample are captured with a spatial resolution of 1024×380 pixels. During the measurement, the normal of the sample surface was aligned to the optical axis of the imaging spectrometer so that the reflection angles remain at zero. The light source arm rotated around its rotational center to vary the incidence angles θ_i. We captured the interferogram datacubes at the 13 incidence angles, ranging from 15 deg to 70 deg. For simplicity, we only present the BRDF data at the normal reflection direction in this work.

For each interferogram datacube, the interferogram dimension had 512 samples. After the Fourier transformation and the data merging, we obtain a four-dimensional (4-D) spectral reflection dataset, given as $I(x, y, \lambda, \theta_i)$. We have 41 wavelength samples over the working spectrum of the instrument. Therefore, the final spectral reflection data have $1024 \times 380 \times 41 \times 13$ data points. Here, we can extract the image of the sample surface at $\lambda = 300$ nm and $\theta_i = 18$ deg as an example and present the image in Fig. 4(a). After applying the spectral calibration and the BRDF normalization, the dataset is transformed into the spectral SVBRDF

$f_r(x, y, \lambda, \theta_i)$. One pixel in Fig. 4(a) is chosen, which is marked by an asterisk, to illustrate the obtained spectral BRDF data on this surface point. The spectral BRDFs of this surface point are presented in Fig. 4(b). Note that the obtained reflection spectra of the aluminum alloy are slight different from that of pure aluminum, which is monotonically increasing from 200 to 400 nm.

The spectral SVBRDF $f_r(x, y, \lambda, \theta_i)$ shows both spectral and angular variations of BRDF at each pixel on the image plane. The data are useful for many applications, such as trace detection, latent image detection, and material characterization. For these applications, the spectral images at several angular configurations are usually sufficient. As long as the spectra of different material are distinctive, it is possible to classify the pixels of these materials. When the data in the spectral dimension are not sufficient to do so, one more dimension of the measurement data in the angular domain becomes useful. In addition, the materials of a sample surface might have different highlights. The signal–noise ratio could be very low at a certain angular configuration, therefore, more samples in the angular domain are important here.

5.2 Surface Characterization

Here, we show how to use this dataset for rough surface characterization. To partition the pixels into two different surfaces according to their surface roughness, we use the k-means algorithm to analyze the SVBRDF data. The spectral BRDF data at each pixel $f_r(\lambda, \theta_i)$ (a 41×13 matrix) are converted into a vector of 533 elements, so that the SVBRDF data construct a data space of 533 dimensions. The distance in this data space is defined as the squared Euclidean distance between the two data points. Assuming two cluster centroids, the k-means algorithm is implemented to minimize the overall distance between these data points and the two cluster centroids.

The results of the clustering are presented in two difference colors, as presented in Fig. 5(a). Although some noise is present, Fig. 5(a) shows reasonable clustering results of the
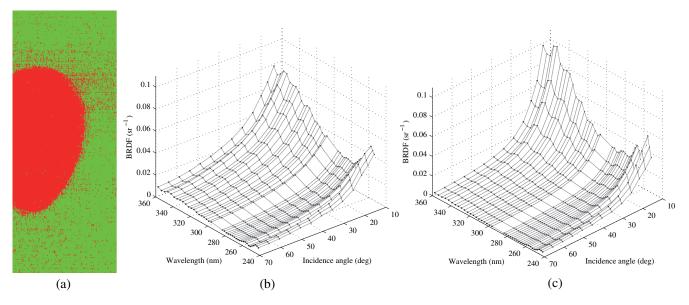
Fig. 5 Clustering results of spectral SVBRDF data: (a) the clustering result, (b) cluster centroid of green pixels, and (c) cluster centroid of red pixels.

Table 1 The fitting results of the Torrance–Sparrow BRDF model.

Surface regions	ρ_d	ρ_s	m
Green	0.0012 ± 0.0004	0.0298 ± 0.0127	0.153 ± 0.007
Red (logo)	0.0009 ± 0.0002	0.0285 ± 0.0096	0.192 ± 0.006

pixels. Since the roughness distribution of the sample surface is simple, we are able to manually separate the logo region from the rest of the surface with Photoshop® and to mark the pixels in these two regions. By doing so, the error of the clustering can be estimated by comparing the actual distribution to the clustering results. It was found that the mismatched pixels are 3.9% of all the pixels. The two obtained cluster centroids, which are the means of all the spectral BRDF data $f_r(\lambda, \theta_i)$ in each cluster, are given in Figs. 5(b) and 5(c). The two spectral BRDFs show similar spectra but different variation trends with incidence angles.

We fit the Torrance–Sparrow BRDF model to the two cluster centroids (or mean BRDF). The model was developed to model the light scattering of metallic surfaces based on the geometrical optics.[23] For the fitting results of all 41 wavelengths, we calculate their means and standard deviations. The two sets of fitting results are summarized in Table 1, where ρ_d and ρ_s are the mean coefficients of the diffuse and specular reflection, respectively, and m is the mean RMS slope.

The fitting results show that the coefficients of the diffuse and specular reflection are close for both surface regions; the RMS slope m of the red (logo) region is about 4/3 of that of the rest of the surface. This implies that the logo region is rougher than the rest of the surface. m shows a standard deviation less than 5%, implying a consistent fitted m over the work band of the instrument. On the other hand, the coefficients of the diffuse reflection ρ_d show a large standard deviation. The results are consistent with the reflective spectra as shown in Figs. 5(b) and 5(c), where the reflection spectra vary with the wavelength.

The mean BRDF data and the fitted curves of three wavelengths, which are 250.9, 319.2, and 349.8nm, are compared in Figs. 6(a) and 6(b), showing a good agreement between the theoretical model and the measurement data. The fitted curves are presented as solid lines. Figures 6(a) and 6(b) show the mean BRDFs of green pixels and red (logo) pixels,
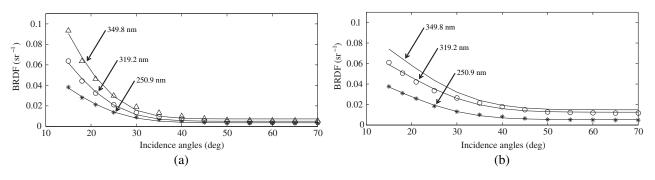

Fig. 6 Comparison of measured BRDF and fitted BRDF at three wavelengths and the normal reflection direction: (a) fitting results of green pixels and (b) fitting results of red pixels.

respectively. For the BRDF data obtained from a single pixel, more deviation can be observed when compared with the fitted curves.

6 Conclusion

In this work, we present a BRDF measurement instrument and experimentally demonstrate that it is able to capture spatially varying multispectral BRDF data in the near- and middle-UV bands. For the presented instrument, the maximum number of pixel numbers is 1024×1024 pixels and the spatial resolution is ~ 50 μm on the sample surface. This enables the proposed instrument to measure a small sample with good spatial resolution. The imaging spectrometer is able to provide 41 samples in the wavelength ranges of 240 to 285 nm and 295 to 370 nm. Thus the spectral resolution is ~ 3 nm. The proposed instrument allows the incidence angle to vary from 10 deg to 90 deg with 0.1 deg resolution. In practice, it is very hard to obtain the BRDF data at grazing angles due to the large projection area of the light source. Therefore, we limit the angular range of incidence angle from 12 deg to 75 deg. The 0.1 deg angular resolution is sufficient for rough surface characterization, but to analyze optical components such as mirrors requires better angular resolutions. The dynamic range of the camera (FLI Proline PL4710) of the imaging spectrometer is estimated to be slightly less than 1:10000. By combining each of several exposures with different integration times, we are able to extend the dynamic range of the BRDF measurement to about 3 orders of magnitudes. A lower detector temperature with a long exposure time might further extend the dynamic range. However, a longer exposure time (>10 s) becomes prohibitive since to capture one interferogram datacube demands hundreds of exposures.

The spectral SVBRDF $f_r(x, y, \lambda, \theta_i)$ could become a very large dataset if dense samples are taken in the spatial, spectral, and angular dimensions. Ideally, the instrument is able to capture 4-D spectral SVBRDF dataset of $1024 \times 1024 \times 41 \times 630$ 16-bit data, which is about 50 GBytes. Although we only present the BRDF data of the normal reflection ($\theta_r = \varphi_r = 0$), the sample holder allows different reflection angles, which can add one more angular dimension to the measured BRDF. A five-dimensional spectral SVBRDF dataset $f_r(x, y, \lambda, \theta_i, \theta_r)$ can easily exceeds terabytes. In practice, only a limited number of samples are needed for each sampling dimension, depending on the application scenario.

One major drawback of this design is the long acquisition time. To capture a datacube of hundreds of images demands a long capture time (from minutes to hours), and many datacubes are needed for sufficient sampling in the angular dimension. Currently, the entire data acquisition process is semiautomatic, since the rotational stage needs to be adjusted manually. Although the manual adjustment only takes seconds, which is not significant compared to the long capture time of a datacube, it does require extra effort and constant attention from the users. This also prevents taking a large number of samples in the angular domain. The spectral scope of the BRDF measurement is also limited. So far only the middle- to near-UV band is allowed. Although the film coated on the scanning mirror filters out the incidence light in the visible spectral range, it also narrows the incidence spectrum in UV the range. Using the PTFE panel

as the reference sample for BRDF normalization might bring error in the instrument parameter $\kappa(\lambda)$. We estimate the error is not more than 5% by examining the available BRDF data in the publication.[22]

The multidimensional BRDF data contain valuable information of the sample surfaces and materials. The angular dimension of the data enables us to separate the surface regions with similar spectral characteristics but with different roughness characteristics or different scattering characteristics. With the development of pattern recognition algorithms, such multidimensional data can be analyzed to recover latent spatial or spectral characteristics of the surface materials. The data and the data analysis methods presented in this paper exhibit great potential in many application fields. In the future, a motor-driven rotation stage will be added to enable BRDF measurement of an anisotropic surface. The control system will also be upgraded to facilitate the data acquisition process.

References

1. J. Li and R. K. Y. Chan, "Toward a UV-visible-near-infrared hyperspectral imaging platform for fast multiplex reflection spectroscopy," *Opt. Lett.* **35**(20), 3330–3332 (2010).
2. F. G. France, "Advanced spectral imaging for noninvasive microanalysis of cultural heritage materials: review of application to documents in the U.S. Library of Congress," *Appl. Spectrosc.* **65**(6), 565–574 (2011).
3. H. Lyu et al., "High resolution ultraviolet imaging spectrometer for latent image analysis," *Opt. Express* **24**(6), 6459–6468 (2016).
4. P. Y. Barnes and J. J. Hsia, "UV bidirectional reflectance distribution function measurements for diffusers," *Proc. SPIE* **1764**, 285–288 (1993).
5. T. F. Schiff et al., "Design review of a high-accuracy UV to near-IR scatterometer," *Proc. SPIE* **1995**, 121–130 (1993).
6. T. H. Zurbuchen, P. A. Bochsler, and F. Scholze, "Reflection of ultraviolet light at 121.6 nm from rough surfaces," *Opt. Eng.* **34**(5), 1303–1315 (1995).
7. M. P. Newell et al., "Extreme ultraviolet scatter from particulate-contaminated mirrors," *Proc. SPIE* **2541**, 174–185 (1995).
8. M. P. Newell and R. A. M. Keski-Kuha, "Bidirectional reflectance distribution function of diffuse extreme ultraviolet scatterers and extreme ultraviolet baffle materials," *Appl. Opt.* **36**(22), 5471–5475 (1997).
9. S. Schröder et al., "Angle-resolved scattering and reflectance of extreme-ultraviolet multilayer coatings: measurement and analysis," *Appl. Opt.* **49**(9), 1503–1512 (2010).
10. G. T. Georgiev and J. J. Butler, "Long-term calibration monitoring of spectralon diffusers BRDF in the air-ultraviolet," *Appl. Opt.* **46**(32), 7892–7899 (2007).
11. L. Bai et al., "Seven-parameter statistical model for BRDF in the UV band," *Opt. Express* **20**(11), 12085–12094 (2012).
12. L. Bai et al., "Spectral scattering characteristics of space target in near-UV to visible bands," *Opt. Express* **22**(7), 8515–8524 (2014).
13. K. J. Dana et al., "Reflectance and texture of real-world surfaces," *ACM Trans. Graphics* **18**(1), 1–34 (1999).
14. K. J. Dana and J. Wang, "Device for convenient measurement of spatially varying bidirectional reflectance," *J. Opt. Soc. Am. A* **21**(1), 1–12 (2004).
15. Y. Dong et al., "Manifold bootstrapping for SVBRDF capture," *ACM Trans. Graphics* **29**(4), 98 (2010).
16. M. Aittala, T. Weyrich, and J. Lehtinen, "Practical SVBRDF capture in the frequency domain," *ACM Trans. Graphics* **32**(4), 1 (2013).
17. D. B. Goldman et al., "Shape and spatially-varying BRDFs from photometric stereo," *IEEE Trans. Pattern Anal.* **32**(6), 1060–1071 (2010).
18. J. M. Medina et al., "Detailed experimental characterization of reflectance spectra of *Sasakia charonda* butterfly using multispectral optical imaging," *Opt. Eng.* **53**(3), 033111 (2014).
19. G. J. Edelman, T. G. van Leeuwen, and M. C. Aalders, "Visualization of latent blood stains using visible reflectance hyperspectral imaging and chemometrics," *J. Forensic Sci.* **60**(S1), S188–S192 (2015).
20. T. Dubroca, G. Brown, and R. E. Hummel, "Detection of explosives by differential hyperspectral imaging," *Opt. Eng.* **53**(2), 021112 (2014).

21. A. Makrushin, T. Scheidat, and C. Vielhauer, "Capturing latent fingerprints from metallic painted surfaces using UV–VIS spectroscope," *Proc. SPIE* **9409**, 94090B (2015).
22. A. Bhandari et al., "Bidirectional reflectance distribution function of spectralon white reflectance standard illuminated by incoherent unpolarized and plane-polarized light," *Appl. Opt.* **50**(16), 2431–2442 (2011).
23. K. E. Torrance and E. M. Sparrow, "Theory for off-specular reflection from roughened surfaces," *J. Opt. Soc. Am.* **57**, 1105–1114 (1967).

Hongsong Li received his BS degree in optoelectronic engineering from Beijing Institute of Technology in 1994, his MS degree in engineering mechanics from Tsinghua University in 1998, and his PhD from Cornell University in 2005. He is an associate professor at the School of Software, Beijing Institute of Technology. His current research interests include optical measurement, computational photography, augmented reality, and computer graphics.

Hang Lyu received BS, MS, and PhD degrees from the School of Optoelectronics, Beijing Institute of Technology. He is currently with the Faculty of Forensic Science Institute of People's Public Security University of China. His research interests include imaging spectrometer and applications on the process of hyperspectral data.

Ningfang Liao received his BS, MS, and PhD degrees from Beijing Institute of Technology and did his postdoctoral research from 1999 to 2001 at Tsinghua University. He is a professor at the School of Optoelectronics, Beijing Institute of Technology. His research interests include style imaging spectrometer, spectroscopy, color science, and technology of digital color.

Wenmin Wu received his BS and MS degrees from Beijing Institute of Technology. He is a faculty member in the School of Optoelectronics, Beijing Institute of Technology. He is currently pursuing his PhD in optical engineering from the same school. His research interests include spectroscopy, color vision, and color management systems.